A Broadband High-Gain Fabry-Perot Cavity Antenna for Vehicle-to-Everything Applications

M. M. Ulfah[1], P. Janpugdee[1,2], D. Torrungrueng[3], and H.-T. Chou[4]

[1]Department of Electrical Engineering, Faculty of Engineering, Chulalongkorn University, Bangkok, Thailand.

[2]Wireless Network & Future Internet Research Unit, Faculty of Engineering, Chulalongkorn University, Bangkok, Thailand.

[3]Research Center of Innovation Digital and Electromagnetic Technology, Department of Teacher Training in Electrical Engineering, Faculty of Technical Education, King Mongkut's University of Technology North Bangkok, Bangkok, Thailand.

[4]Graduate Institute of Communication Engineering, National Taiwan University, Taipei, Taiwan.

Corresponding author: Panuwat Janpugdee (panuwat.ja@chula.ac.th)

Key Points:

- A broadband antenna is integrated with a partially reflective surface consisting of two dielectric slabs for wideband gain enhancement.
- The positive phase gradient of the PRS can be achieved by appropriately selecting the thickness of the slabs and the size of the air gap.
- The proposed PRS improves the antenna gain by up to 5 dB.

Abstract

In this paper, a Fabry-Perot cavity (FPC) antenna with a partially reflective surface (PRS) consisting of two dielectric slabs with identical thickness and permittivity to increase the gain with wide bandwidth is presented. The PRS is placed in front of a broadband U-shaped microstrip patch antenna to create an air-filled cavity between the PRS and the ground plane of the antenna structure. The configuration of the two dielectric slabs aims to create a positive phase gradient of the reflection coefficient, which strongly controls the gain bandwidth performance. The proposed PRS was first designed and analyzed using a transmission line model and then verified by a full-wave simulation. The measurement results show that the proposed FPC antenna achieves a gain improvement of up to 5 dB compared to the antenna without PRS, with a 3-dB gain bandwidth of 11.5% and a broadside peak gain of 9.88 dBi. In addition, the measured impedance bandwidth is approximately 18.8% and ranges from 4.95–6 GHz, which covers the required frequency band for vehicle-to-everything (V2X) applications.

Plain Language Summary

A new design of a broadband antenna with high gain has been developed by using two identical dielectric slabs placed in front of a broadband microstrip patch. This antenna is intended for vehicle-to-everything (V2X) communications. The proposed configuration increases the degrees of freedom and design flexibility to improve the antenna gain over a wide frequency range. The proposed antenna is more practical as it is compact, lightweight, and easy to fabricate.

1 Introduction

The popularity of smart transportation has led to the development of vehicular wireless communication systems, with vehicle-to-everything (V2X) emerging as a significant development in enhancing connectivity and communication capabilities within the advancement of transportation technology. In conjunction with the advanced driver assistant system (ADAS), V2X will enhance safety as well as situational awareness, optimizing traffic efficiency, and overall transportation effectiveness. There are two different standards for V2X communications, namely the WLAN-based standard and the cellular-based standard. The WLAN-based standard refers to IEEE 802.11p designed specifically for V2X communications operating in the 5 GHz band, while for the cellular-based standard, e.g., cellular vehicle-to-everything (C-V2X) operating at the frequency of 5.9 GHz.

A highly directive antenna is required to provide high antenna gain for strong signal strength, a longer communication range, higher reliability, and better resistance to interference. These features are essential to ensure reliable communication between vehicles and infrastructure for safety enhancement. However, conventional high-gain antennas, such as reflectors, Yagi-Uda, and array antennas, possess large and complex physical configurations and are thus unsuitable for vehicular applications. Recently, the Fabry-Perot cavity (FPC) antennas garnered the attention of many researchers due to their good characteristics, such as high efficiency, high gain, and simple feeding technique. The concept of FPC antennas was first proposed in 1956 (Trentini, 1956), where a PRS is placed in front of the source or feed antenna with a ground plane. The PRS is positioned at a certain distance from the ground plane of the source antenna to create an air cavity in between. The electromagnetic (EM) waves produced by the radiating antenna will undergo multiple reflections within the cavity. This process results in an in-phase superposition of associated EM waves if the resonant conditions are satisfied. Consequently, highly directive radiation is formed.

The conventional design of FPC has a narrow gain bandwidth (BW) because of its resonant characteristics. Several approaches have been proposed to broaden the gain BW. A single-layer unprinted dielectric substrate with a transverse permittivity gradient (TPG) was used to overcome the bandwidth limitation (Hashmi & Esselle, 2016; Baba, Hashmi, & Esselle, 2017). In Ji, Qin, & Guo (2017), by utilizing a flat ground plane at the center and angularly tilting it upwards in a trapezoid shape at the corner, the 3-dB gain bandwidth of the proposed antenna has been increased to 20.2%. These methods effectively improve the gain BW but suffer from complex design and fabrication processes. Another common technique uses a PRS with a positive phase gradient. This type of response can be obtained using a frequency-selective surface (FSS), which can be classified as a printed PRS. Two-layer PRSs consisting of hexagonal and tripod branch unit cells were employed for size reduction and to make the FPC antenna more compact, achieving a peak gain of 14.2 dBi and 3-dB gain BW of 34.2% (Guan et al., 2021). Using two types of FSS unit cells arranged in a chessboard pattern on a single-layer substrate to create a hybrid PRS (HPRS) was reported (Liu et al., 2020). The hybrid surface (HS) and reflective surface (RS) are formed by employing cross and square ring-shaped patches, which results in a measured peak gain of 17.08 dBi and a 3-dB gain BW of 25.4%. A complementary unit cell design was also proposed to provide a positive phase gradient (Wang et al., 2014; Lian, Tang & Yin, 2018; Meriche et al., 2019). Subsequently, multilayer dielectric slabs, classified as unprinted PRSs, were also used to obtain a positive phase gradient (Zeb et al., 2012; Al-Tarifi et al., 2013; Wang et al., 2015). A combination of multiple thin dielectric slabs arranged closely together was reported (Nguyen-Trong et al., 2018). The thicknesses are only $0.1\,\lambda_{\mathrm{subs}}$ (λ_{subs} is the dielectric wavelength at the center frequency). These slabs were separated by a $0.1\lambda_0$ (λ_0 is the free space wavelength) air gap. The measured maximum gain is 14.2 dBi, and the 3-dB gain bandwidth is up to 86%.

The aforementioned literature has demonstrated that the unprinted PRS exhibits superior performance in terms of gain BW enhancement despite its simple structure. Taking the potential of unprinted PRSs in gain enhancement, a broadband and high-gain FPC antenna presented in this paper is intended to work for V2X communications. The antenna configuration consists of PRSs placed over a broadband microstrip patch antenna. The proposed PRS consists of two dielectric substrate slabs with an equal thickness and dielectric constant; they are separated by an air cavity. The PRS reflection coefficient with a positive phase gradient improves gain performance over a wide frequency range.

The rest of this paper is organized as follows. Section 2 presents the design and analysis of the PRS. The antenna design and simulation results are illustrated in Section 3. In Section 4, the measurement results are shown, and the proposed work is compared with some competing designs in the literature. Finally, conclusions are provided in Section 5.

2 PRS Design and Analysis

A PRS is a surface that reflects part of the incident EM waves while transmitting the rest. In antenna applications, the PRS is placed in front of the feed antenna to control the radiated EM wave and improve the radiation performance of the antenna. The properties of PRSs have a strong influence on the radiation characteristics of the antenna, such as gain, radiation pattern, and operating BW. The PRS and the ground plane, which is usually part of the feed antenna, form an air cavity in which multiple reflections of EM waves occur. The mechanism for improving the antenna gain is based on the resonance of the EM waves in the cavity. The most important property of the PRS is its complex reflection coefficient ($\Gamma_{PRS} = |\Gamma_{PRS}|\, e^{j\phi_{PRS}}$). The reflection phase

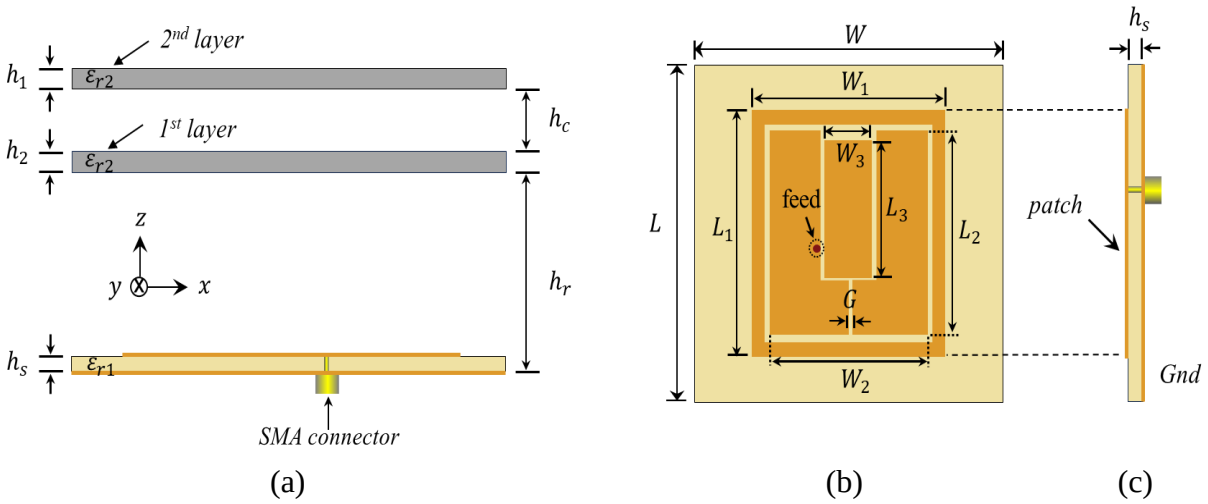

Figure 1. Design of the proposed antenna. (a) cross-section view (b) top-view of feed antenna (c) side-view of feed antenna.

(ϕ_{PRS}), or the phase of the reflection coefficient, of the PRS for a resonant condition of the cavity in the broadside direction of the antenna (perpendicular to the PRS) can be expressed as follows (Trentini, 1956):

$$\phi_{PRS} = \frac{4\pi h_r}{\lambda_0} + 2N\pi + \phi_{GND}, \quad (1)$$

where $N = 0, \pm1, \pm2, \ldots$, ϕ_{GND} is the phase of the reflection coefficient of the ground plane, and h_r is the height of the air cavity between the PRS and the ground plane. From (1) it can be seen that a positive phase gradient of the PRS reflection coefficient over a wide frequency range is required to achieve a wide gain BW of the FPC antenna.

The PRS structure can consist of a variety of materials, including dielectrics, metals, or combinations thereof. One of the simplest PRS structures consists only of dielectric substrates (unprinted PRS). The functional mechanism of the PRS can be described using analytical methods such as the transmission line (TL) model. Using the TL model can show that a single-layer dielectric PRS should be half a wavelength thick to achieve the desired reflection phase characteristics (Nguyen-Trong et al., 2018). However, opting for this thickness leads to an unwieldy antenna. In addition, the desired thickness of substrate for the operating frequency range may not be commercially available.

The configuration of the FPC antenna presented in this work is shown in Figure 1. The proposed PRS consists of two layers of dielectric substrates with the same thickness ($h_1 = h_2$) and dielectric constant (ε_{r2}), separated by an air gap (h_c). The use of a two-layer PRS leads to more degrees of freedom and offers more flexibility in the design process. Several variables can be varied to achieve the desired reflection properties of the PRS, i.e., the dielectric constant and the thickness of the substrate as well as the height of the air gap. Given the unavailability of a particular material thickness in the market, modifying the air cavity height will be more convenient than altering the substrate thickness.

The two dielectric substrates used in the present design are Rogers RT/duroid 6010LM (ε_r= 10.2) with a thickness of 1.9 mm ($0.11\lambda_g$), where λ_g is the wavelength in the substrate at the

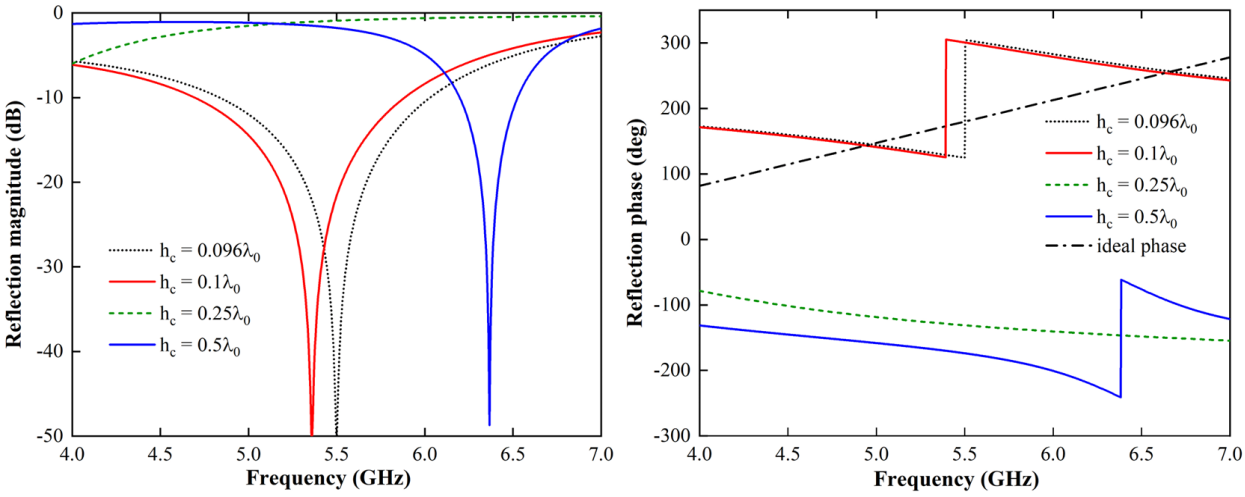

(a) (b)

Figure 2. Reflection coefficients of the proposed PRS with different heights of the air gap calculated with the TL model. (a) magnitude (b) phase.

center frequency. The height of the air gap (h_c) is properly chosen to obtain a positive phase gradient. Figure 2 shows the reflection coefficients calculated with the TL model for the proposed PRS with different heights of the air gap. Also shown is a plot of the ideal positive phase gradient, which intersects with the plots of the reflection coefficient phase. It can be seen that the positive phase gradient intersects with the ideal phase at the resonant frequency when the height of the air gap is set to $0.096\lambda_0$ (5.17 mm).

To verify the preliminary design by the TL model, the proposed PRS structure is also simulated with CST Studio Suite (Dassault Systèmes, 2021). It is modeled as a periodic unit cell, as shown in Figure 3, to simplify the simulation. The magnitude and phase of the reflection coefficients obtained using CST Studio Suite and the TL model are compared in Figure 3. It can be seen that both results agree very well.

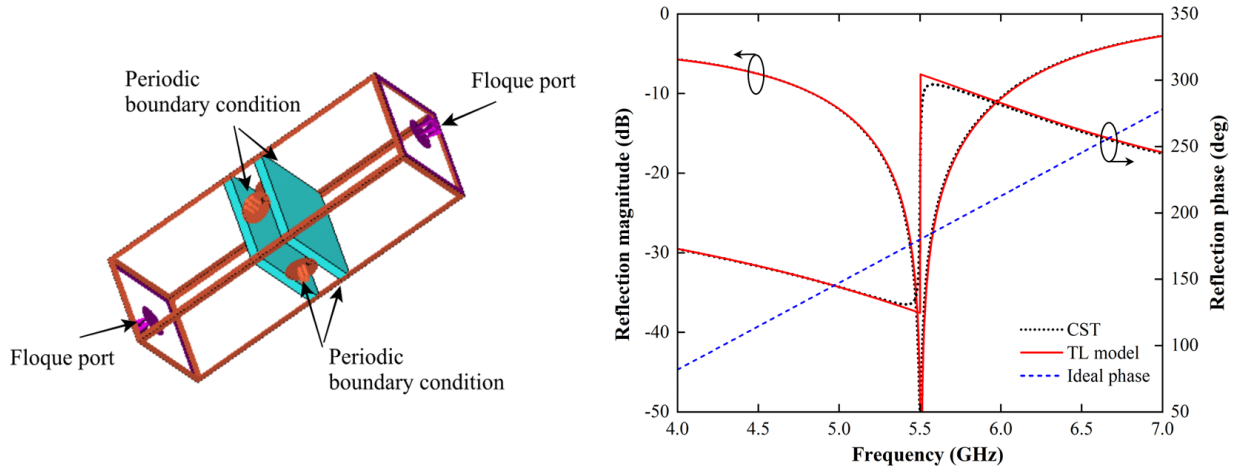

(a) (b)

Figure 3. (a) Unit cell model of the proposed PRS in the simulation. (b) reflection coefficients of the proposed PRS determined by CST Studio Suite and the TL model.

It has been demonstrated in this section that by carefully choosing the thickness of the substrate and the air gap, the phase response can exhibit a positive gradient and intersect with the ideal phase given on the right-hand side (RHS) of (1) over a wide frequency band. Note that, with the proposed PRS, the positive phase gradient can be obtained with a more compact structure, namely $0.11\lambda_g + 0.095\lambda_0 + 0.11\lambda_g$.

3 Antenna Design and Characterization

The proposed FPC antenna configuration consists of two main parts: a feed antenna and the PRS. The feed antenna plays an important role in determining the performance of the designed antenna. The directivity of the feed antenna contributes to the achieved directivity of the FPC antenna as described by the following equation (Niaz et al., 2021):

$$D_{FPCA} = D_{feed} + D_{PRS,} \tag{2}$$

where D_{FPCA} is the directivity of FPC antenna, D_{feed} and D_{PRS} are the feed antenna and PRS directivities, respectively.

In this paper, the microstrip patch antenna is used as the feed antenna because it is known for its outstanding features such as low cost, low profile, planar structure, and easy fabrication. The microstrip patch antenna is printed on the FR-4 substrate (ε_{r1}= 4.3) with a thickness (h_s) of 1.6 mm. The 50-ohm coaxial probe is used to feed the antenna through the SMA connector. The design evolution of the microstrip antenna and their simulated reflection coefficient magnitude ($|S_{11}|$) results are given in Figure 4.

Note that Ant_1 consists of a U-shaped patch to obtain a wide impedance BW ($|S_{11}| \leq -10$ dB). This antenna generates two resonant modes, namely TM_{20} (5 GHz) and TM_{21} (5.9 GHz). The introduction of a slot into the structure (Ant_2) causes the second resonance TM_{02} (5.7 GHz) to appear and is combined with a rectangular patch (Ant_3) placed in the center of the U-shaped patch. This configuration creates a multimode resonance, resulting in a wide impedance BW. Finally, Ant_4 is designed by adding the rectangular ring to further broaden the impedance BW. The final design of the microstrip antenna exhibits an impedance BW range from 4.969 to 6.001 GHz (18.96%), aligning perfectly with the frequency band requirements for V2X applications.

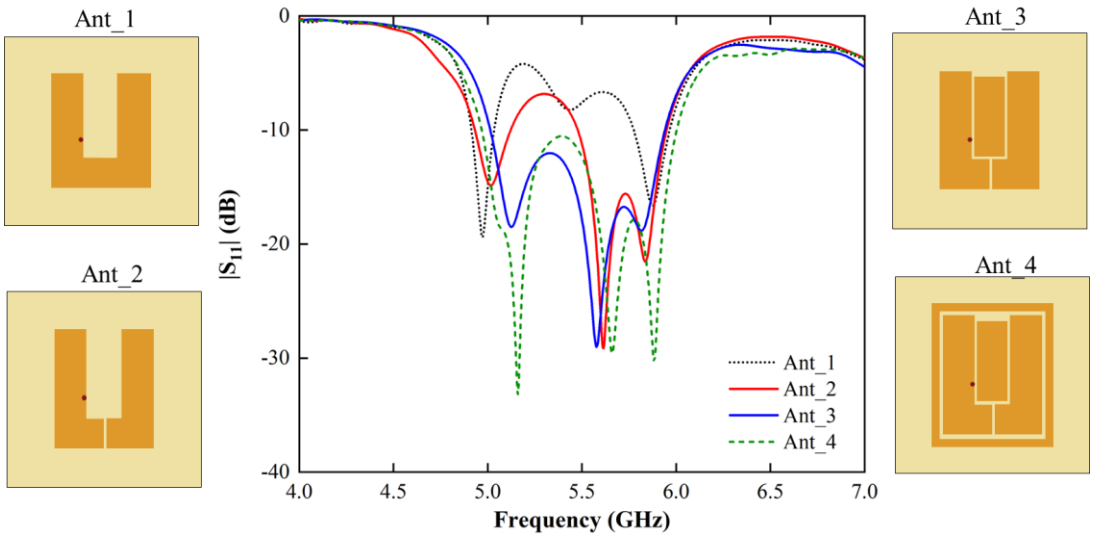

Figure 4. Geometry evolution of the microstrip antenna and its simulated $|S_{11}|$.

The designed PRS is then integrated into the feed antenna. The FPC is formed by the PRS and the ground plane of the feed antenna. The reflection phase of PRS is known from the simulation results, and the reflection coefficient of the ground plane (assuming PEC) is approximately –1. Therefore, the height of the FPC between the PRS and the ground plane (h_r) can be determined using (1). With $\phi_{PRS} = 221.76^{o}$, $\phi_{GND} \approx 180^{o}$, and $N = 0$, $h_r = 30.44$ mm is obtained. However, to enhance the gain performance of the FPC antenna, the cavity height (h_r) was further optimized using CST Studio. Figure 5 shows the |S11| and broadside gain characteristics when h_r is varied. After the optimization, it is found that $h_r = 28.67$ mm is the optimum value. The geometric parameters of the proposed FPC antenna are listed in Table 1.

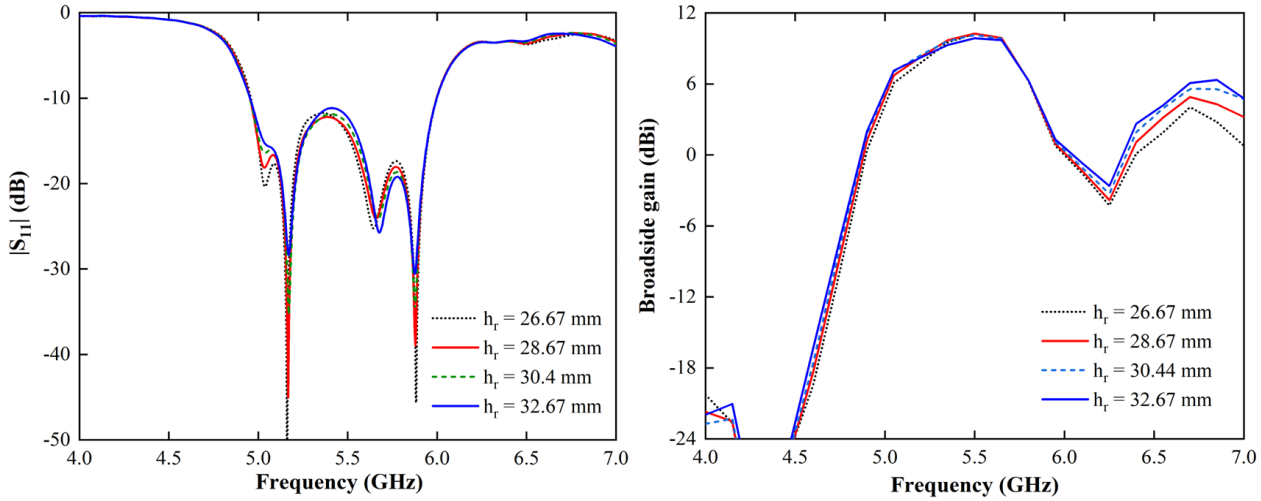

(a) (b)

Figure 5. Performances of the proposed antenna with values of h_r varied. (a) simulated |S11| (b) simulated broadside gain.

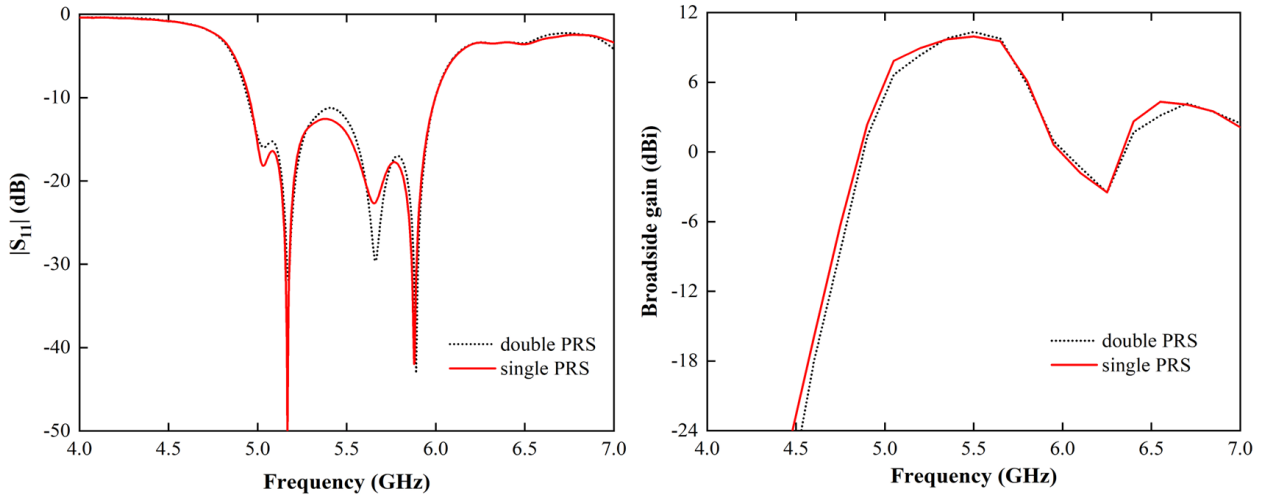

(a) (b)

Figure 6. Comparison of the proposed antenna with single-layer PRS. (a) simulated |S11| (b) simulated broadside gain.

Table 1 *Geometric Parameters of The Proposed FPC Antenna.*

Parameters	Values (mm)	Parameters	Values (mm)	Parameters	Values (mm)
L	60	W_2	25	h_1	1.9
W	60	L_3	19.5	h_2	1.9
L_1	36	W_3	8	h_r	28.67
W_1	32	G	1	h_c	5.17
L_2	28	h_s	1.6	–	–

A half-wavelength thickness of single-layer PRS is compared with the proposed double-layer PRS. The single-layer PRS has a thickness of 8.5 mm, whilst the proposed double-layer PRS has an overall thickness of 8.8 mm (including air gap). The thicknesses are almost equal. However, the proposed PRS is lighter. As seen, the performances of simulated $|S_{11}|$ and broadside gain are very similar to each other as plotted in Figure 6.

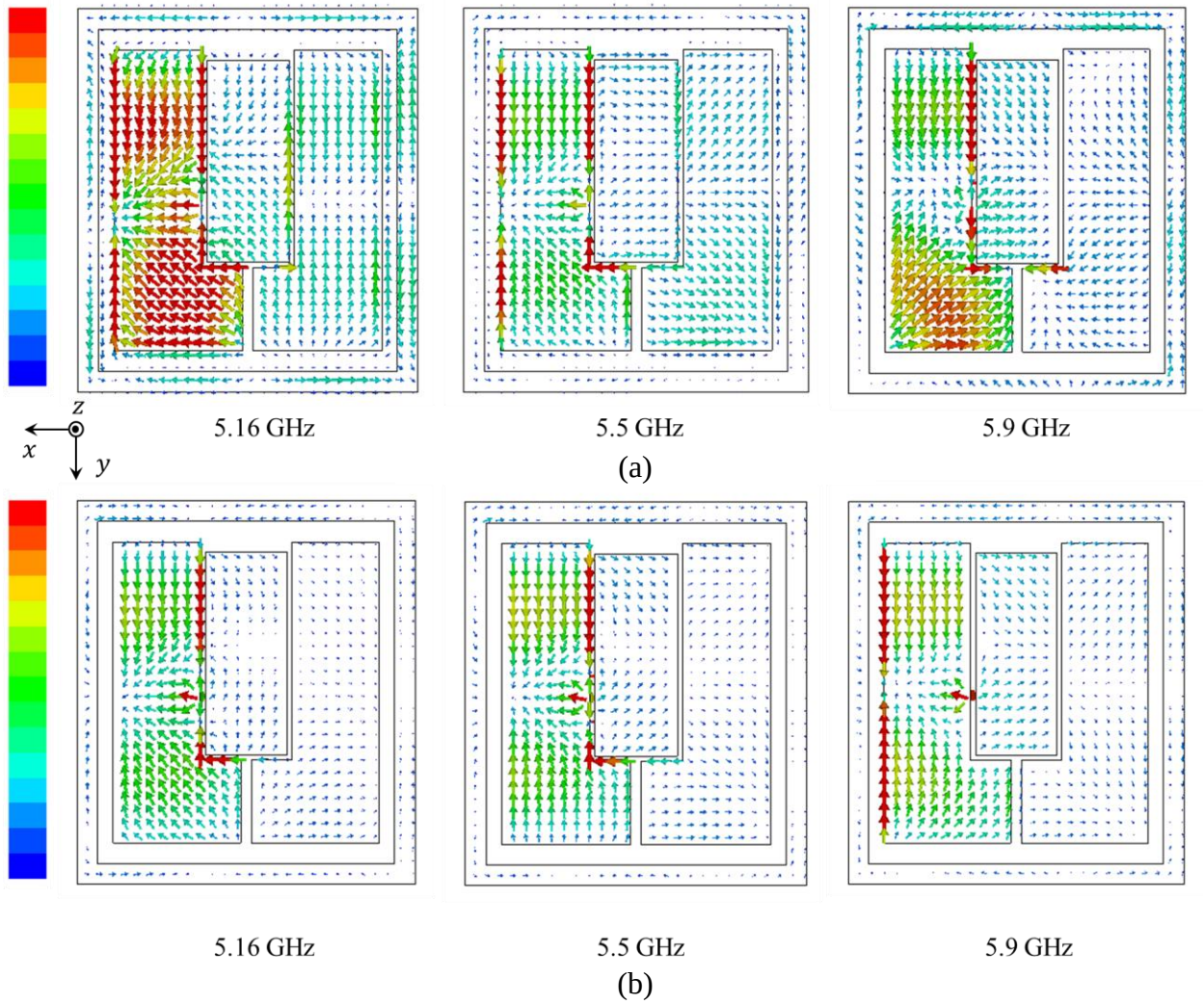

Figure 7. Surface current distribution at three resonant frequencies. (a) feed antenna (without the PRS) (b) feed antenna with the PRS.

Figure 7 shows the surface current distribution on the metallic portion of the antenna at three resonant frequencies. The introduction of the PRS in the feed antenna significantly affects the current distribution. The PRS can alter the EM environment around the antenna, leading to changes in the way current flows on the antenna structure. The reflective properties of the PRS affect the phase and amplitude of the EM waves, which in turn, can impact the impedance matching, radiation pattern, and overall performance of the feed antenna.

4 Results and Discussions

To validate the simulation results, the proposed FPC antenna is then fabricated where the prototype is given in Figure 8(a). The nylon is used to support the PRS layers and create an air cavity. The measurements were performed in an anechoic chamber as shown in Figure 8(b).

The comparison of simulated and measured $|S_{11}|$ is depicted in Figure 9(a), where the −10 dB impedance BW for the feed antenna (without the PRS) is 18.82% (4.969−6.001 GHz), and 18.64% (4.963−5.983 GHz) with respect to the center frequency, respectively. Additionally, it can be seen that the simulated −10 dB impedance BW for the antenna with PRS is 19.02% (4.954−5.995 GHz), and the measured one is 18.80% (4.95−5.977 GHz). In Figure 9(b), the presence of PRS significantly increases the broadside gain of the feed antenna from 4.85 to 9.88 dBi, with a 3-dB gain BW of 11.5% in the measured result, while the simulated result is from 5.89 to 10.32 dBi with 11.74% of 3-dB gain BW. Overall, the simulated and measured results are in good agreement. The slight discrepancies may be caused by fabrication errors, uncertainty of material properties, and soldering issues.

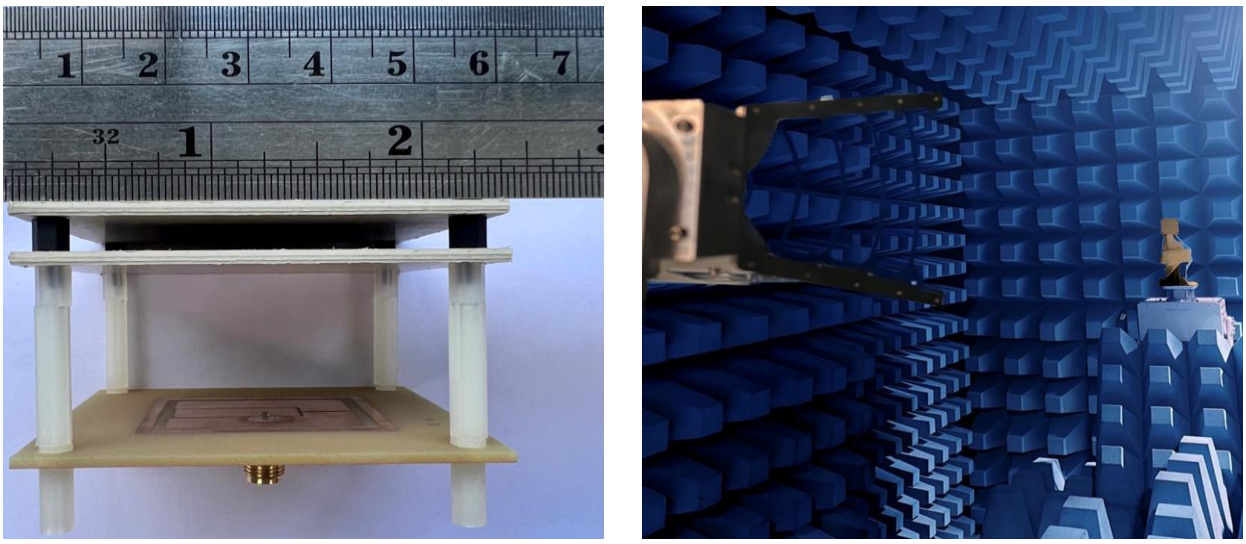

(a) (b)

Figure 8. (a) Fabricated FPC antenna (b) radiation measurement set-up.

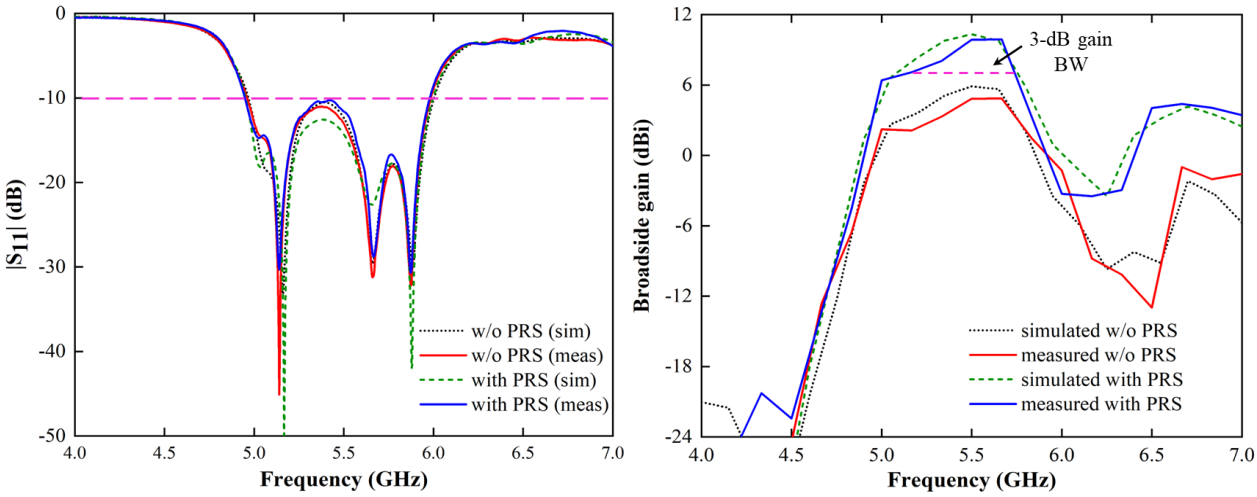

(a) (b)

Figure 9. The comparison between simulated and measured results of the FPC antenna. (a) $|S_{11}|$ (b) broadside gain.

The simulated and measured radiation patterns of the proposed antenna at 5.16, 5.5, and 5.9 GHz are plotted in Figure 10. It can be observed that the main beam orientation of the FPC antenna is in the broadside direction at three distinct frequencies in the H−plane, while at 5.9 GHz the main beam orientation is slightly tilted in the E–plane. It is noteworthy that since the antenna excitation is not symmetric in the E– and H–planes, the antenna has an asymmetric radiation pattern in both planes.

Table 2 compares the performance of the proposed FPC antenna with some previous works of vehicular antennas in the literature. It can be seen that the proposed antenna has a comparatively high gain and a fairly wide BW with a relatively compact size. It also has a simple structure with only a single feed and is easy to fabricate.

Table 2 *Comparison between the Proposed FPC Antenna and Reported Antennas.*

References	f_{min} (GHz)	Size ($\lambda_{f_{min}}$ *)	IBW (%)	Max. gain (dBi)	3-dB gain BW (%)	Num. of layers	Rad. pattern type
(Sufian et al., 2022)	5.61	1.38 × 1.38 × 0.03	7.05	7.68	N/A	1	Directional
(Xing et al., 2022)	4.82	3.2 × 2.41 × 0.08	27.6	4.2	7.8	1	Directional
(Sun, Leung, & Lu, 2021)	5.3	0.53 × 0.35 × 0.11	41.6	8.46	10.3	2	Directional
(Gao et. al., 2018)	5.42	3.07 × 3.07 × 0.08	9.8	7.5	N/A	2	Omni-directional
(Wong, So & Gao, 2016)	4.82	1.03 × 1.03 × 0.05	32.2	6.5	32.25	1	Omni-directional
This work	**4.95**	**0.99 × 0.99 × 0.62**	**18.80**	**9.88**	**11.5**	**3**	Directional

*$\lambda_{f_{min}}$ is the free-space wavelength at the lowest frequency of the bandwidth.

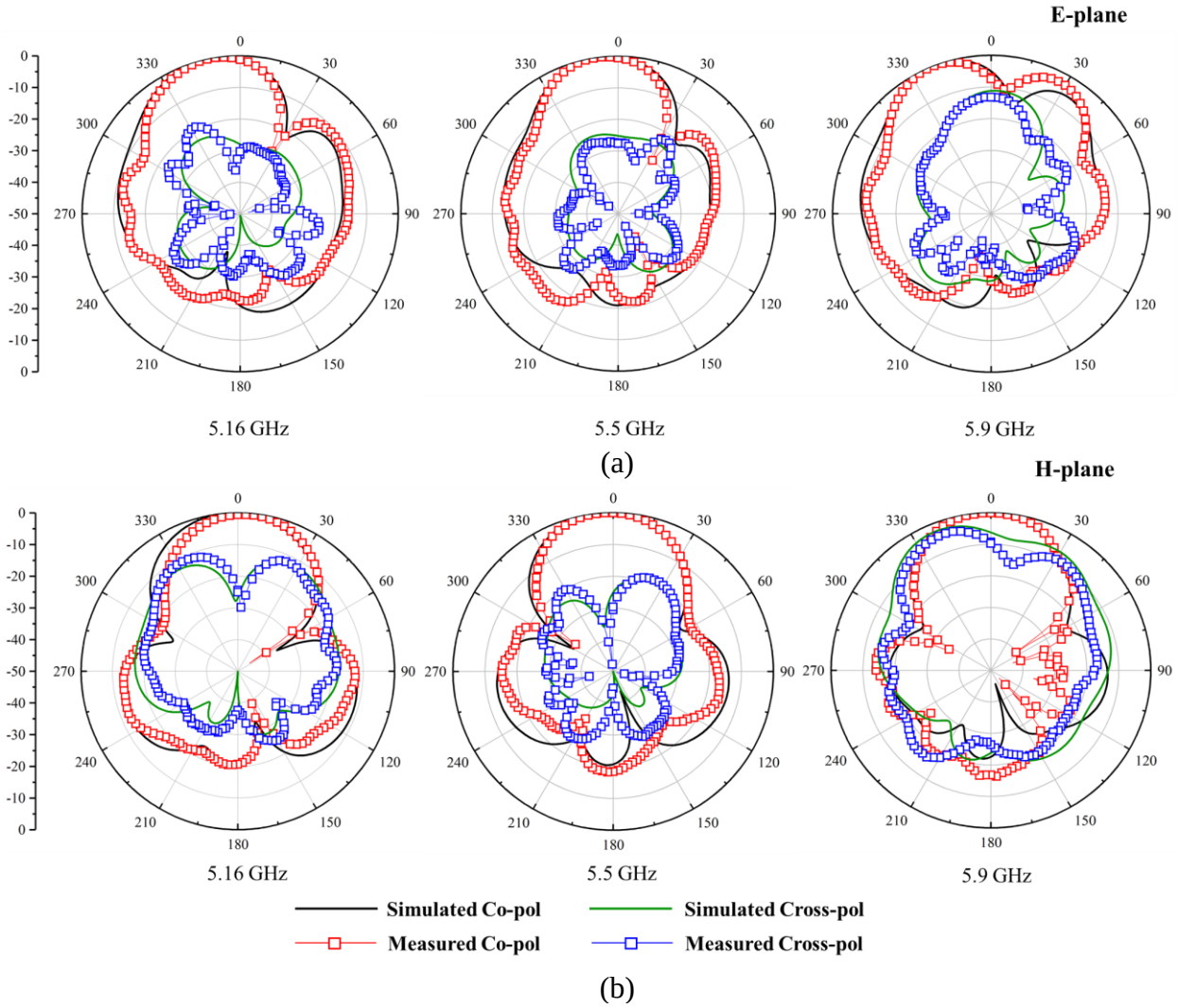

Figure 10. Simulated and measured radiation patterns of the FPC antenna at 5.16 GHz, 5.5 GHz, and 5.9 GHz. (a) E–plane (b) H–plane.

5 Conclusions

This paper presents a broadband high-gain FPC antenna for V2X communications. The gain-bandwidth performance is achieved through the appropriate design of the PRS reflection coefficient that exhibits a positive phase gradient. The proposed PRS is readily realized by two dielectric substrates with the same dielectric constant and thickness separated by an air gap with a suitable height. This structure is relatively practical since it is compact, lightweight, and easy to fabricate. The measurement results show that the proposed PRS can effectively increase the gain of the feed antenna with wide gain BW. In addition, a novel asymmetric PRS design based on compact microstrip resonant cells (CMRCs) is currently investigated for future works. Experimental characterizations of this novel PRS design are still in progress, where the measurement results will be reported later.

Acknowledgments

This research was funded in parts by (i) Ratchadapisek Somphot Fund for Wireless Network & Future Internet Research Unit, Chulalongkorn University [Contract no. GRU 6409521015-1], (ii) National Science, Research and Innovation Fund (NSRF), King Mongkut's University of Technology North Bangkok [Project no. KMUTNB-FF-67-A-04], and (iii) The Ministry of Science and Technology, Taiwan.

References

Al-Tarifi, M. A., Anagnostou, D. E., Amert, A. K., & Whites, K. W. (2013). Bandwidth enhancement of the resonant cavity antenna by using two dielectric superstrates. *IEEE Transactions on Antennas and Propagation,* 61(4), 1898-1908. DOI: 10.1109/TAP.2012.2231931

Baba, A. A., Hasmi, R. M., & Esselle, K. P. (2017). Achieving a large gain-bandwdith product from a compact antenna. *IEEE Transactions on Antennas and Propagation,* 65(7), 3437−3446. DOI: 10.1109/TAP.2017.2700016

Dassault Systèmes. (2021). *CST Studio Suite 2021, Dassault Systèmes.* Retrieved from: https://www.3ds.com/products-services/simulia/products/cst-studio-suite/solvers/

Gao, S., Ge, L., Zhang, D., & Qin, W. (2018). Low-profile dual-band stacked microstrip monopolar patch antenna for WLAN and car-to-car communications. *IEEE Access*, 6, 69575−69581. DOI: 10.1109/ACCESS.2018.2877420

Guan, Y., Jiao, Y-C., Yan, Y-D., Feng, Y., Weng, Z., & Tian, J. (2021). Wideband and compact Fabry–Perot resonator Antenna using partially reflective surfaces with regular hexagonal unit. *IEEE Antennas and Wireless Propagation Letters*, 20(6), 1048-1052. DOI: 10.1109/LAWP.2021.3070376

Hashmi, R. M., & Esselle, K. P. (2016). A class of extremely wideband resonant cavity antennas with large directivity-bandwidth products. *IEEE Transactions on Antennas and Propagation,* 64(2), 830−835. DOI: 10.1109/TAP.2015.2511801

Ji, L-Y., Qin, P-Y., & Guo, Y. J. (2018). Wideband Fabry-Perot cavity antenna with a shaped ground plane. *IEEE Access*. 6. 2291−2297. DOI: 10.1109/ACCESS.2017.2782749

Lian, R., Tang, Z., & Yin, Y. (2018). Design of a broadband polarization-reconfigurable Fabry-Perot resonator antenna. *IEEE Antennas and Wireless Propagation Letters,* 17(1), 122−125. DOI: 10.1109/LAWP.2017.2777502

Liu, Z., Liu, S., Zhao, X., Kong, X., Huang, Z., & Bian, B. (2020). Wideband gain enhancement and RCS reduction of Fabry-Perot antenna using hybrid reflection method. *IEEE Transactions on Antennas and Propagation,* 68(9), 6497−6505. DOI: 10.1109/TAP.2020.2988949

Meriche, M. A., Attia, H., Messai, A., Mitu, S. S. I., & Denidni, T.A. (2019). Directive wideband cavity antenna with single-layer meta-superstrate. *IEEE Antennas and Wireless Propagation Letters,* 18(9), 1771−1774. DOI: 10.1109/LAWP.2019.2929579

Nguyen-Trong, N., Tran, H. H., Nguyen, T. K., & Abbosh, A. M. (2018). Wideband Fabry-Perot antennas employing multilayer of closely spaced thin dielectric slabs. *IEEE Antennas and Wireless Propagation Letters,* 17(7), 1354−1358. DOI: 10.1109/LAWP.2018.2846240

Niaz, M. W., Yin, Y., Bhatti, R. A., Cai, Y-M., & Chen, J. (2021). Wideband Fabry-Perot resonator antenna employing multilayer partially reflective surface. *IEEE Transactions on Antennas and Propagation,* 69(4), 2404−2409. DOI: 10.1109/TAP.2020.3022555

Pozar, D. M. (2011). Microwave Engineering, 4th ed., John Wiley & Sons Inc. ISBN: 978-0-470-63155-3

Sufian, M. A., Hussain, N., Abbas, A., Lee, J., Park, S. G., & Kim, N. (2022). Mutual Coupling Reduction of a Circularly Polarized MIMO Antenna Using Parasitic Elements and DGS for V2X Communications. *IEEE Access*, 10, 56388−56400. DOI: 10.1109/ACCESS.2022.3177886.

Sun, Y-X., Leung, K. W., & Lu, K. (2021). Compact dual microwave/millimeter-wave planar shared-aperture antenna for vehicle-to-vehicle/5G communications. *IEEE Transactions on Vehicular Technology*, 70(5), 5071−5076. DOI: 10.1109/TVT.2021.3070353

Wang, N., Liu, Q., Wu, C., Talbi, L., Zeng, Q., & Xu, J. (2014). Wideband Fabry-Perot resonator antenna with two complementary FSS layers. *IEEE Transactions on Antennas and Propagation,* 62(5), 2463−2471. DOI: 10.1109/TAP.2014.2308533

Wang, N., Li, J., Wei, G., Talbi, L., Zeng, Q., & Xu, J. (2015). Wideband Fabry–Perot resonator antenna with two layers of dielectric superstrates. *IEEE Antennas and Wireless Propagation Letters*, 14. 229-232. DOI: 10.1109/LAWP.2014.2360703

Wong, H., So, K. K., & Gao, X. (2016). Bandwidth enhancement of a monopolar patch antenna with V-shaped slot for car-to-car and WLAN communications. *IEEE Transactions on Vehicular Technology,* 65(3), 1130−1136. DOI: 10.1109/TVT.2015.2409886

Xing, X-Q., Lu, W-J., Ji, F-Y., Zhu, L., & Zhu, H-B. (2022). Low-profile dual-resonant wideband backfire antenna for vehicle-to-everything applications. *IEEE Transactions on Vehicular Technology,* 71(8), 8330−8340. DOI: 10.1109/TVT.2022.3175258

Zeb, B. A., Ge, Y., Esselle, K. P., Sun, Z., & Tobar, M. E. (2012). A Simple Dual-Band Electromagnetic Band Gap Resonator Antenna Based on Inverted Reflection Phase Gradient. *IEEE Transactions on Antennas and Propagation,* 60(10), 4522−4529. DOI: 10.1109/TAP.2012.2207331